


# Evolution of Renal-Disease Factor APOL1 Results in *Cis* and *Trans* Orientations at the Endoplasmic Reticulum That Both Show Cytotoxic Effects

Daria Müller,<sup>1</sup> Jürgen Schmitz ,<sup>2</sup> Katharina Fischer,<sup>1</sup> Daniel Granado,<sup>1</sup> Ann-Christin Groh,<sup>1</sup> Vanessa Krausel,<sup>1</sup> Simona Mareike Lüttgenau,<sup>1</sup> Till Maximilian Amelung,<sup>1</sup> Hermann Pavenstädt,<sup>1</sup> and Thomas Weide\*,<sup>1</sup>

<sup>1</sup>Internal Medicine D (MedD), Molecular Nephrology, University Hospital of Münster (UKM), Münster, Germany

<sup>2</sup>Institute of Experimental Pathology, ZMBE, University of Münster, Münster, Germany

\*Corresponding author: E-mail: weidet@uni-muenster.de.

Associate editor: Harmit Malik

## Abstract

The recent and exclusively in humans and a few other higher primates expressed *APOL1* (apolipoprotein L1) gene is linked to African human trypanosomiasis (also known as African sleeping sickness) as well as to different forms of kidney diseases. Whereas *APOL1*'s role as a trypanolytic factor is well established, pathobiological mechanisms explaining its cytotoxicity in renal cells remain unclear. In this study, we compared the *APOL* family members using a combination of evolutionary studies and cell biological experiments to detect unique features causal for *APOL1* nephrotoxic effects. We investigated available primate and mouse genome and transcriptome data to apply comparative phylogenetic and maximum likelihood selection analyses. We suggest that the *APOL* gene family evolved early in vertebrates and initial splitting occurred in ancestral mammals. Diversification and differentiation of functional domains continued in primates, including developing the two members *APOL1* and *APOL2*. Their close relationship could be diagnosed by sequence similarity and a shared ancestral insertion of an *AluY* transposable element. Live-cell imaging analyses showed that both expressed proteins show a strong preference to localize at the endoplasmic reticulum (ER). However, glycosylation and secretion assays revealed that—unlike *APOL2*—*APOL1* membrane insertion or association occurs in different orientations at the ER, with the disease-associated mutants facing either the luminal (*cis*) or cytoplasmic (*trans*) side of the ER. The various pools of *APOL1* at the ER offer a novel perspective in explaining the broad spectrum of its observed toxic effects.

**Key words:** *APOL1*, *APOL2*, endoplasmic reticulum, evolutionary medicine, *APOL* gene family, *APOL* phylogeny, *APOL* selection analyses, kidney disease.

## Introduction

*APOL1* (apolipoprotein L1) is the most-studied variant of six members of conserved human proteins (*APOL1-6*) and has been identified as a trypanolytic factor (TLF) by protecting humans against African sleeping sickness causing *Trypanosoma* parasites (Hajduk et al. 1989; Raper et al. 1999; Vanhamme et al. 2003; Pays et al. 2014; Weckerle et al. 2016). *Trypanosoma brucei rhodesiense* and *Trypanosoma brucei gambiense* subspecies are resistant to *APOL1* and escaped from *APOL1* toxicity. By a coevolutionary arms race, two variants of *APOL1*—G1 (S342G/I384M) and G2 (Δ388N, Δ389Y)—reestablished the *APOL1*-linked protection against these parasites in humans of sub-Saharan African ancestry (Pays et al. 2014; Capewell et al. 2015; Kruzel-Davila, Wasser, et al. 2017). The *APOL1* variant G2 lyses *Trypanosoma brucei rhodesiense*, but not *Trypanosoma brucei gambiense*, whereas *APOL1*-G1 is associated with latent, asymptomatic infections

in those infected with *Trypanosoma brucei gambiense* (Cooper et al. 2017).

However, similar to the link between sickle cell anemia and human resistance to malaria, two copies of these variants cause an increased risk for numerous renal, predominantly glomerular, diseases (Freedman et al. 2010; Genovese et al. 2010; Kasembeli et al. 2015). These include HIV- and hypertension-associated nephropathy, focal segmental glomerulosclerosis, lupus nephritis, membranous nephropathy, and—as recently shown—also Covid-19-associated renal failure (Tzur et al. 2010; Kopp et al. 2011; Papeta et al. 2011; Larsen et al. 2014; Velez et al. 2020). These diseases' common features include proteinuria and rapidly progressive kidney disease, which often results in end-stage renal disease (Wiggins 2007). Therefore, podocytes—unique postmitotic cells, essential for the glomerular filtration barrier establishment and maintenance—are most likely a primary cellular

target for APOL1-associated renal cytotoxicity (Wiggins 2007; Kopp et al. 2020).

All APOL family members share high sequence homology. In a concept initially suggested by Pays and colleagues for APOL1 (Perez-Morga et al. 2005; Pays et al. 2006), and extended to all APOL family members by Smith and Malik (2009), APOL proteins contain three functional parts: a pore-forming domain (PFD), a membrane addressing domain (MAD), and SRA-interacting-protein-like domain (SID). The PFD of APOLs include Bcl-2 homology 3 (BH3) domain-like sequence motifs (BSMs) that have been linked to anti- or pro-apoptotic features (Wei et al. 2001; Shamas-Din et al. 2011; Dummer et al. 2015; Adams and Cory 2018). A further common feature of the APOL family is that their expression can be induced by inflammatory triggers, for example, interferons or TNF $\alpha$ , indicating that they are part of the innate immune system (Vanhollebeke and Pays 2006; Zhaorigetu et al. 2008, 2011; Liao et al. 2011; Nichols et al. 2015). APOL1 is only expressed in humans and a few other higher primates. It is the only APOL family member containing an N-terminal signal peptide (SP) mediating its secretion into the serum as a TLF (Duchateau et al. 1997; Pays et al. 2006; Friedman and Pollak 2011).

In contrast, numerous studies provide evidence that the increased risk for renal diseases is caused by intracellular and therefore noncirculating pools of APOL1 (Chen et al. 2015; Heneghan et al. 2015; Khatua et al. 2015; Ma et al. 2017, 2020; Olabisi et al. 2016; Beckerman et al. 2017; Granado et al. 2017; Kruzel-Davila, Shemer, et al. 2017; Madhavan et al. 2017; Shah et al. 2019; Uzureau et al. 2020). The observation that reduced kidney allograft survival is linked to the donor's and not the recipient's genotype supports this (Reeves-Daniel et al. 2011; Lee et al. 2012; Freedman et al. 2015, 2016). Of note, APOL2–6 lack SPs, suggesting that common or evolutionarily conserved properties of APOLs are most likely linked to intracellular functions.

Thus, considering evolutionary aspects combined with in silico prediction tools and cell biological experiments may help us obtain more in-depth insights into the pathobiological details of APOL1-associated cell injury.

## Results

### APOL1 and APOL2 Are the Most Recent Members of a 300-Ma-Old Gene Family

We reconstructed the genomic locus of the APOL gene family and included for the first time the gene *APOLD1* (from apolipoprotein L domain containing 1), which shows modest homology (~30% identity) to the central part of human APOL6 (BSM and membrane insertion domain/MID) on protein level (Regard et al. 2004). The *APOLD1* sequence is highly conserved and shows 88% identity (92% similarity) versus mouse *APOLD1* and 62% identity (75% similarity) versus *APOLD1* from chicken. It is present in all mammals and can be traced back 300 Ma to an amniote ancestry. The high *APOLD1* similarity in deep vertebrate splits indicates strong functional constraints (fig. 1).

APOL6 and APOL5 are represented in most placental species. However, the mouse genome lacks APOL5. All other investigated APOL gene family members are significantly younger and either primate or rodent specific (Page et al. 2001; Smith and Malik 2009; Kreit et al. 2015). Our data suggest a rodent-primate APOL6-like ancestor gene origin about 70 Ma (fig. 1B, supplementary data SD1–3, Supplementary Material online) that—after duplication—diverged independently into numerous APOL genes in man and mouse. Thus, mice (mm: *Mus musculus*) contain 13 APOL genes that can be divided into *mmAPOLD1*, *mmAPOL6*, an *mmAPOL7* group (*mmAPOL7a*, *7b*, *7c*, and *7e*), *mmAPOL8*, an *mmAPOL9* group (*mmAPOL9a*, *9b*), and an *mmAPOL10/11* group (*mmAPOL10a*, *10b*, *11a*, *11b*). All these genes are clustered on chromosome 15 except *mmAPOLD1*, which is located on chromosome 6. The human (hs: *Homo sapiens*) *APOLD1* is localized on chromosome 12, and human APOL1–6 genes are clustered on chromosome 22 (fig. 1, supplementary data SD1–3, Supplementary Material online, and Smith and Malik 2009).

To verify the protein sequence-based reconstruction and derive some information about splitting times of APOL genes in humans, we aligned the entire genomic sequences of the human APOL1–6 cluster and searched for phylogenetically informative transposed elements. These elements were inserted before splitting of different gene members. Therefore, orthologous transposons shared among the various duplicated APOL genes reveal their close evolutionary relationships. Furthermore, based on the age of the inserted diagnostic elements and their species distribution, they provide information about the timeframe of duplication and diversification (Kuryshv et al. 2006).

This approach provided an additional perspective on the evolution of APOL gene families and resulted in the identification of two phylogenetically diagnostic, primate-specific *Alu* SINEs (short interspersed elements) in the human APOL gene cluster: *AluJ* and *AluY*. The shared diagnostic *AluJ* element was detected in the intronic region of all investigated primates at orthologous positions in APOL1–4 and was probably inherited from a common primate ancestor about 70 Ma. Only APOL1 and APOL2 shared the diagnostic *AluY* element in the 5' untranslated region (UTR). The orthologous *AluY* transposon was already present in Catarrhine primates that diverged about 30 Ma (for dating, see Churakov et al. [2010]). Thus, the common *AluY* motif indicates a close relationship between APOL2 and APOL1.

The APOL1 splice variants correspond to the terminology suggested by Khatua et al. (2015). Figure 2 presents the cumulated exon composition of APOL1 isoforms compared with APOL2–4 and includes the positions of diagnostic *AluJ* and *AluY* insertions which are absent in APOL6, APOL5, and *APOLD1*. In addition, our studies revealed traces of a MER41G long terminal repeat element in APOL1–4 genes. They lead to a new alternative transposable element exon (TE exonization) and transcription termination in the APOL4 gene (fig. 2, supplementary data SD4, Supplementary Material online).

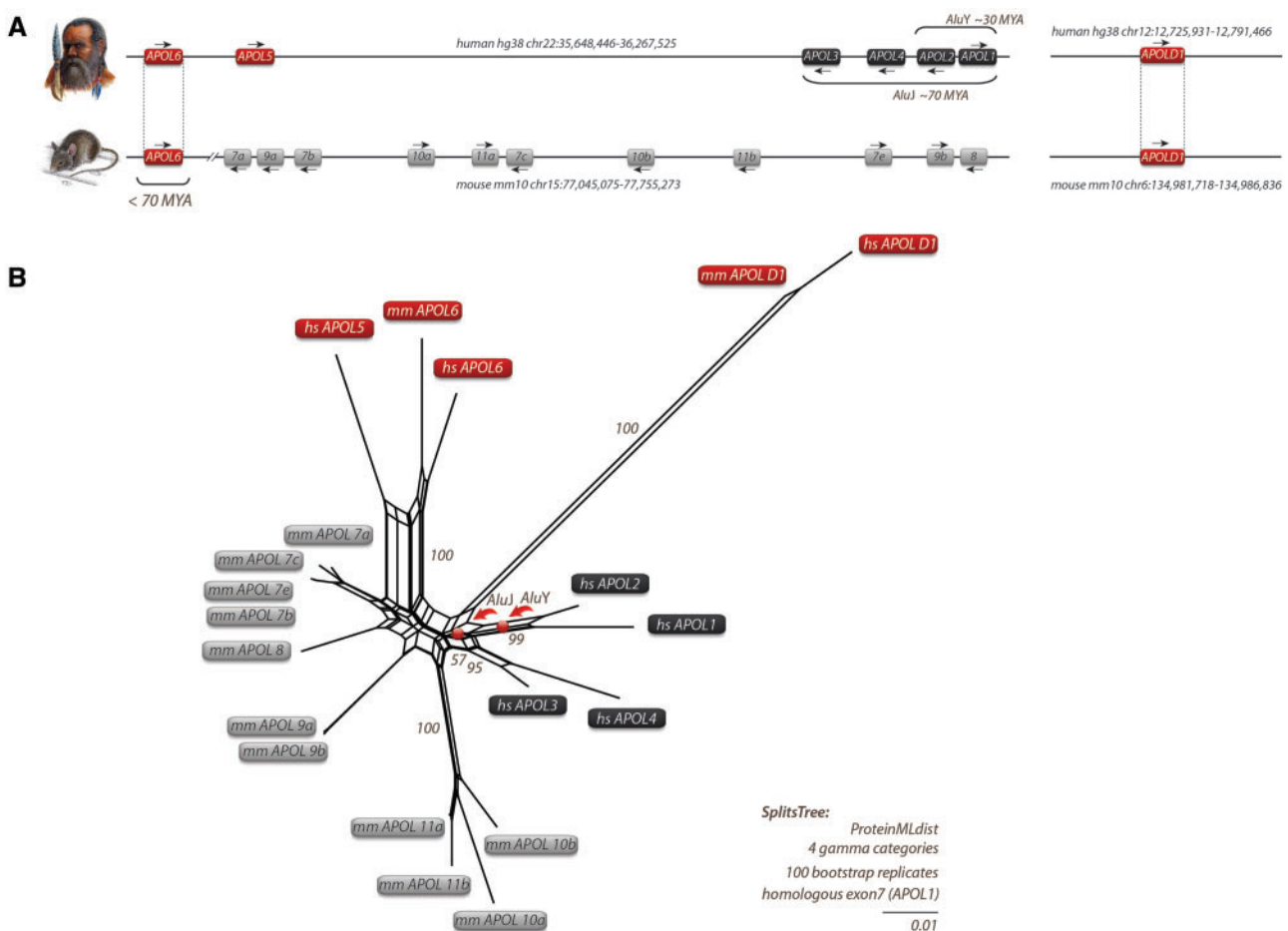


**Fig. 1.** Local APOL gene family and SplitsTree reconstructions for humans and mice. (A) Genomic location of APOL genes from human and mouse with genomic coordinates. Arrows indicate gene orientations. APOLD1 evolved early in vertebrates about 300 Ma, whereas APOL6 was probably inherited by a human–mouse ancestor that lived about 70 Ma. (B) SplitsTree reconstruction of APOL genes based on protein sequences. A similar tree topology was derived by maximum likelihood and Bayesian tree reconstructions (supplementary data SD1, Supplementary Material online). The APOL genes of mice (mm for *Mus musculus*) are indicated in gray boxes. Black boxes represent human APOL genes (hs for *Homo sapiens*). The central parallelograms of the reconstruction represent conflicting phylogenetic signals. The tree reconstruction reveals a common origin of mm and hs APOL6 (red boxes). Bootstrap values are shown for representative branches. Balls indicate the clade-supporting integrations of *AluJ* and *AluY* elements. The human APOL2 and APOL1 genes share an orthologous *AluY* element. The orthologous *AluY* transposons were already present in Catharrine primates (diverged about 30 Ma). The diagnostic *AluJ* elements were detected at orthologous positions in APOL1–4 in all investigated primates and were probably inherited from a common primate ancestor of about 70 Ma. The double-slash in the mouse locus indicates the exclusion of a large genomic region. Human and mouse APOLD1 are located on chromosomes 12 and 6, respectively, and diverged significantly from other APOL genes.

### APOL1 and APOL2 Show Different Expression in Human Organs during Development

Expression patterns during mammalian organ development may provide first hints about the different functions of closely related *AluY*-positive APOL1 and APOL2 genes. In addition, it may give some information on why only APOL1 is linked to human diseases, once as a protective TLF and once as a risk gene for renal diseases. Therefore, we next analyzed the expression patterns of these genes and used a recently established database of developmental transcriptomes of seven organs (cerebrum, cerebellum, liver, heart, kidney, ovary, and testis) across seven species (human, macaque, mouse, rat, rabbit, opossum, and chicken) (Cardoso-Moreira et al. 2019). We only analyzed human transcriptomes of cerebrum, cerebellum, liver, heart, and kidney because they include both,

pre- and postnatal stages. In these organs, APOL1 and APOL2 are predominantly expressed at postnatal stages (fig. 3). At embryonic and prenatal stages, APOLs exhibit no or only background expression.

APOL1 and APOL2 also appear to exhibit organ-specific expression profiles. In cerebrum and cerebellum, APOL2 is the predominantly expressed APOL gene. This was also observed in other transcriptome databases (supplementary data SD5, Supplementary Material online). Its expression increases during the lifespan, whereas APOL1 is only poorly expressed. The predominant APOL gene in the liver is APOL1 (fig. 3, supplementary data SD5, Supplementary Material online). Its expression is dramatically induced after birth and is maintained at a very high level (~80 reads per kilobase transcript per million [RPKM]). APOL2 also exhibits robust postnatal

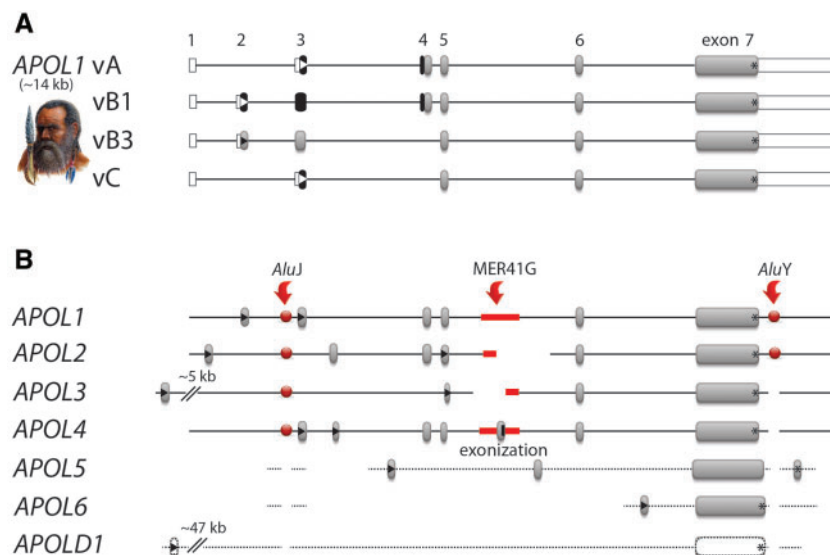


**Fig. 2.** APOL1 isoforms and related APOL gene members. (A) Gene structures of the four well-characterized APOL1 isoforms vA, vB1, vB3, and vC (Khatua et al. 2015). Exons for APOL1 vA (gene size ~14 kb) are labeled 1–7. White frames indicate UTRs, black boxes represent leading SPs, gray boxes the remaining protein-coding exons, and black lines the intronic regions. Start codons are indicated by triangles and stop codons by asterisks. (B) Cumulative gene structures of all human APOL gene members and isoforms. Red arrows indicate the insertion points of three diagnostic transposable elements (*Alu*) merging APOL1–4, MER41G representing alternative exon insertion/exonization in APOL4, *AluY* indicating a common ancestry of APOL1–2). Highly diverged sequences are shown by dotted lines (annotated alignments are provided as [supplementary data SD4, Supplementary Material](#) online).

expression, but only approximately one-fourth of that of APOL1. In heart, APOL1 and APOL2 expressions are significantly upregulated at postnatal stages. Finally, both genes are highly expressed in the kidney at postnatal stages and 19 weeks postconception. Together, closely related APOL1 and APOL2 show different organ-specific expression patterns.

### APOL1–APOL2 Evolutionary Splitting Leads to Different APOL1 Orientations at the ER

In contrast to APOL2, APOL1 is expressed in different splice variants (vA, vB1, vB3, and vC; [fig. 2](#)). Therefore, we applied live-cell imaging to determine the intracellular distributions of GFP-tagged APOL1 splice variants and APOL2 in immortalized podocytes (AB8 cell line, [fig. 4](#)), and HEK293T cells ([supplementary data SD6–8, Supplementary Material](#) online). In both cell lines, all GFP-tagged APOL1 and APOL2 proteins predominantly co-localized with the ER live-cell imaging dye (ER Tracker, [fig. 4](#)); only in some cells, a meager fraction of APOL1 could also be detected co-localizing with the plasma membrane ([supplementary data SD6, Supplementary Material](#) online). Thus, binding to ER membranes seemed to be an evolutionarily conserved common feature of APOL1 and APOL2, as GFP-tagged APOL3 and APOL4 showed different intracellular distributions ([supplementary data SD7 and SD8, Supplementary Material](#) online).

In contrast to APOL2 (and the other APOLs), APOL1 is the only family member found in the bloodstream, indicating that it is released via the secretory pathway. This requires the complete insertion of the nascent APOL1 polypeptide into the ER lumen mediated by a functional SP on a molecular level. We, therefore, wondered whether all APOL1 splice variants carry functional SPs or whether some variants

failed to be secreted and thus remained on the cytoplasmic side of the ER. To address this, we first focused on the different N-terminal regions of APOL1 splice variants that are unique to APOL1 and utterly absent in all other APOLs, including APOL2. In silico analyses (SignalP, TMHMM) using the first 60 amino acids of the APOL1 splice variants predicting putative SPs or hydrophobic transmembrane regions (TMs) led to ambiguous results. These predictions identified putative SPs or hydrophobic helices either only in APOL1 vA and vC or only in vA and vB1 ([supplementary data SD9, Supplementary Material](#) online). We, therefore, addressed this aspect experimentally and replaced the endogenous SP of the reporter enzyme SEAP (secreted alkaline phosphatase) by the different N-termini of APOL1 splice variants and the well-known SP of HSA (human serum albumin) as a positive control ([fig. 5A and B](#)). Indeed, the SEAP secretion assays ([fig. 5B, supplementary data SD9, Supplementary Material](#) online) demonstrated functional SPs in the N-termini of APOL1 vA, vB1, and vC, similar to secretion positive controls (SEAP or HSA SPs). Only SEAP fused to the N-terminus of APOL1 vB3, and the negative control (SEAP without SP) was not secreted. Thus, alternative splicing of APOL1 results in functional SPs of some but not all variants.

APOL2, APOL1 vB3 ([fig. 4](#)), and APOL1 in which the SP was replaced by GFP ([Granado et al. 2017](#)), are targeted to the ER. These data suggest that the APOL1 ER targeting is due to structural information, independent of the N-terminal SP. Therefore, we wondered, how ER targeting could be conserved among APOL1 and APOL2 proteins and second, how—in the case of APOL1—it might be linked to its cytotoxic effects.



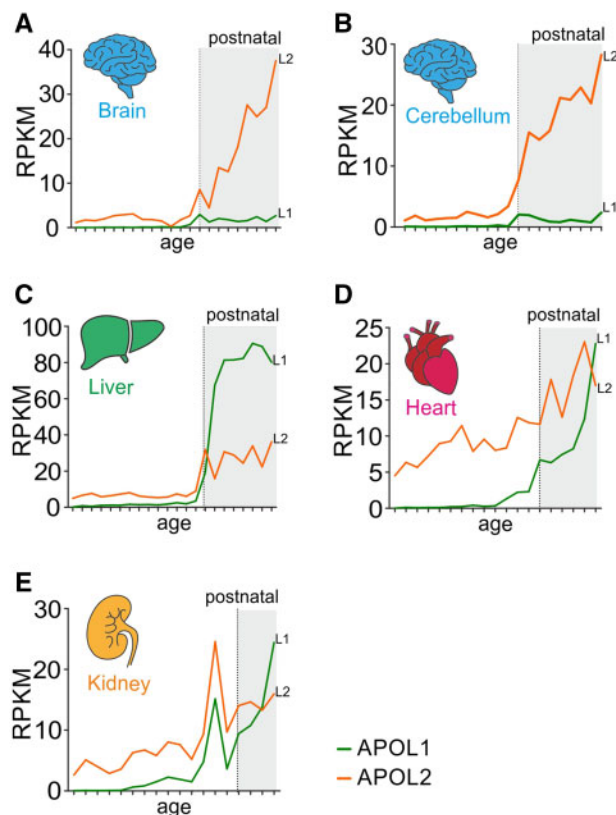


**Fig. 3.** APOL1–APOL2 gene diversification is accompanied by organ-specific expression. (A) Expression levels of APOL1 (L1, green) and APOL2 (L2, orange) transcriptomes (expressed as RPKM-normalized counts) during human organ development derived from the Evo-devo database. White background indicates embryonic or prenatal stages and gray background postnatal stages of mammalian organ development (supplementary data SD20, Supplementary Material online).

In silico analyses using full-length APOL1 (vA) and APOL2 sequences suggest the presence of two to five TMs for APOL1 (including the SP) and two or three TMs for APOL2 (supplementary data SD10–12, Supplementary Material online). The relative positions of the most significant two TMs within the primary structure are very similar between APOL1 and APOL2 (supplementary data SD10–12, Supplementary Material online). We addressed the possible orientations of various APOL1 splice variants and APOL2 in the ER to examine whether their SIDs—which in case of APOL1 carries the renal risk variants—faced the luminal (*cis*) or cytoplasmic side (*trans*). For that purpose, we took advantage of an artificial N-glycosylation tag (GT, Glyco-tag) (Kaup et al. 2011) that only becomes glycosylated in the ER lumen. We fused this tag to the C-termini of various APOL1 splice variants, APOL2, and included an APOL1 mutant lacking the first 59 amino acids of the N-terminus. This  $\Delta$ N59 deletion mutant is very similar to APOL2 and even starts with an almost identical amino acid sequence (fig. 5C). We expressed these GT-tagged APOL proteins in HEK293T cells. Lysates of transfected cells were treated with and without PNGaseF, a glycosidase that completely removes N-glycosylation. A shift on sodium dodecyl sulfate polyacrylamide gel electrophoresis (SDS-

PAGE) when treated with PNGaseF was present only for APOL1 vA, vB1, and vC, demonstrating an N-glycosylation of the C-terminus of these APOL1 splice variants (fig. 5D). The shift was independent of APOL1 SID variants. Thus, APOL1 G0 and the RRVs G1 and G2 have the same orientation in the ER lumen (fig. 5E and F and supplementary data SD13, Supplementary Material online). However, PNGaseF treatment had no effects on GT-tagged APOL1 vB3, APOL1 lacking the complete N-terminus, including the SP ( $\Delta$ N59), APOL2 (fig. 5C–F), or APOL1 protein in which the SP (aa1–28) was replaced by an N-terminal GFP-tag (supplementary data SD13, Supplementary Material online). The GT and GFP-tag (GFP-GT) combination fused to APOL1 and APOL2 at the C-terminus led to the same outcomes (fig. 5E and F and supplementary data SD13, Supplementary Material online). Together, these data align with the SEAP assays and demonstrated a luminal (*cis*) ER localization of the APOL1 SIDs only in splice variants carrying functional SPs.

Of note, the APOL1 mutant  $\Delta$ C305-GFP-GT, which contains an SP but lacks the SID, becomes glycosylated (fig. 5E and F) and localizes to the ER (supplementary data SD14, Supplementary Material online). Furthermore, we also observed a luminal orientation and ER localization for a C-terminally GFP-GT-tagged APOL1 with an APOL2-BSM, and an APOL1–APOL2 chimera carrying the APOL1 SP, the APOL2 PFD and MAD, and the APOL1 SID (supplementary data SD14 and SD15, Supplementary Material online). Thus, our data show that APOL1 can be expressed in two different orientations at the ER, one fraction (vA, vB1, and vC) with the SID localized inside the ER lumen (*cis*) and one (vB3) with the SID facing the cytoplasm (*trans*), like APOL2.

### APOL1 Shows Cytotoxic Effects in Both Orientations

We determined the cytotoxic potential of *cis*- and *trans*-orientated APOL1 (G0 and RRVs). Both, APOL1-GFP which have luminal orientated SIDs as well as GFP-APOL1 (in which the SP was exchanged by GFP), showed reduced cell viability after 24 and 48 h (fig. 6). The reduced cell viability was pronounced with APOL1 renal risk variants (G1 and G2) but was also present with the used African APOL1 G0 haplotype (E150/I228/K255, see Lannon et al. [2019] and supplementary data SD16, Supplementary Material online). In contrast, APOL2 overexpression had no toxic effect (fig. 6).

Since GFP-APOL2 showed the same *trans* ER orientation as GFP-APOL1 (with the toxic RRV G2), we also investigated the BSM roles in *trans*-orientated APOL1 cytotoxicity (and APOL2 nontoxicity). To address this, we modified the APOL1 BSM (NIRRLRALADGVQKV) by mutating its LRALAD core sequence into six alanine residues (NIRRAAAAAAGVQKV; called B<sub>6xAla</sub>) or by changing the BSM of APOL1 into that of APOL2 (HIRKLRLAEVEVQV; B<sub>2</sub>). Strikingly, both modifications led to a loss of APOL1 cytotoxicity (fig. 6B), demonstrating that APOL1 cytotoxicity in *trans* orientation requires the BSM. In addition, APOL1 with the APOL2 BSM maintained its ER membrane targeting, whereas APOL1 with the B<sub>6xAla</sub> sequence showed a cytoplasmic localization (supplementary data SD15, Supplementary Material online). Chimeric APOL2 proteins, carrying the toxic

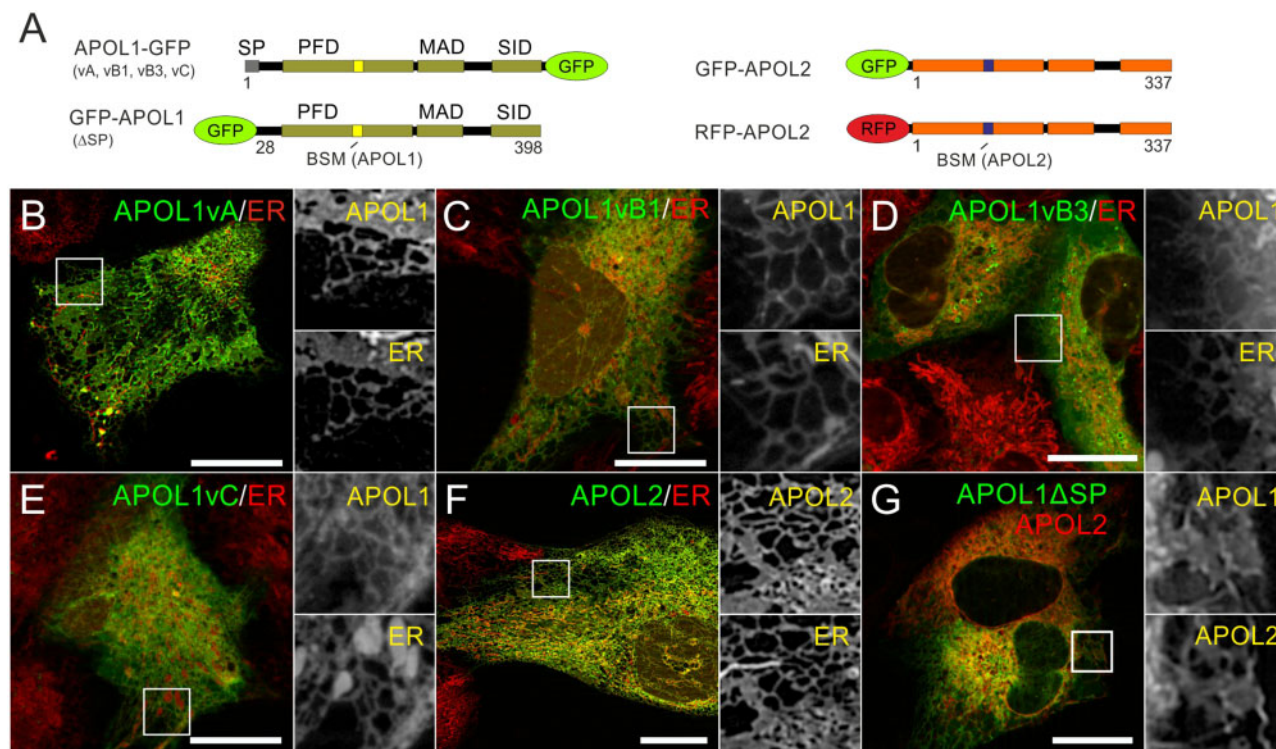


**FIG. 4.** APOL1 splice variants and APOL2 are targeted to the ER. (A) Schemes of C-terminally GFP-tagged APOL1 splice variants, GFP-APOL1 (lacking the SP,  $\Delta$ SP, aa1-27), and N-terminally GFP- or RFP-tagged APOL2. Live-cell imaging of AB8 podocytes, expressing APOL1-GFP splice variants vA, vB1, vB3 and vC (B–E), GFP-APOL2 (F), or GFP-tagged APOL1 together with RFP-APOL2 (G). ER membranes are visualized with live-cell imaging dye ER Tacker. Scale bars: 20  $\mu$ m.

SID of APOL1-G2 ( $P_2M_2S_{1-G2}$ ) or both, the putative pro-apoptotic APOL1 BSM and toxic SID ( $P_2B_1M_2S_{1-G2}$ ), were unable to cause toxic effects (data not shown). Thus, cytotoxicity is unique to APOL1, present for both ER orientations but not transferable to cytoplasmic orientated APOL2.

### Positively Selected Sites of APOL1 Are Localized in Putative TMs

Previous work is suggesting that APOL1-linked cytotoxicity mainly bases on cation channel activity at the plasma membrane (Thomson and Finkelstein 2015; Olabisi et al. 2016; Bruno et al. 2017; Giovinazzo et al. 2020; Schaub et al. 2020). This results in novel topology conceptions for APOL1, in which the SP is followed by up to four additional TMs (Giovinazzo et al. 2020; Gupta et al. 2020; Scales et al. 2020; Schaub et al. 2020). Therefore, we reevaluated codons that are under positive selection during APOL1 evolution. These analyses were performed in PAML (Yang 2007; Xu and Yang 2013) and based on a codon alignment of exon 6 and exon 7 (APOL1 vA equivalents for APOL2–4, supplementary data SD17, Supplementary Material online). By applying site-specific models M2 (selection) versus M1 (neutral) and M8 (selection) versus M7 (neutral), and a branch-site model (labeled 2201), more than 100 potential amino acid sites under positive selection were identified (supplementary data SD17, Supplementary Material online). We selected 27 of them with significant support from at least two investigated models and arranged them with the previously detected

positively selected sites (fig. 7A). Three of the 27 twice supported sites (Y273, E313, Y351) correspond to positively selection positions previously identified by Smith and Malik (2009). Relaxing the stringency to once significantly detected sites (M2, M8, or 2201) revealed an overlap of 17 of the 23 positively selected sites of Smith and Malik (fig. 7A, supplementary data SD17, Supplementary Material online). Strikingly, 15 of the 27 positive selected sites are within or close to two putative TMs (TM3: aa257–276 and TM4: aa332–353, fig. 7, supplementary data SD17 and SD18, Supplementary Material online).

### Discussion

Our evolutionary tree reconstructions elucidate an ancestral APOLD1-like precursor gene as the origin of the entire gene family. In addition, our data show almost entirely independent divergences of the APOL gene families in mouse and human, leading to six further human and 12 further murine APOL genes (fig. 1, supplementary data SD1–3, Supplementary Material online, and Page et al. 2001; Smith and Malik 2009; Kreit et al. 2015). A search for phylogenetically diagnostic primate-specific transposable elements revealed two *Alu* SINEs in the APOL gene family. *AluJ* is located at orthologous positions in APOL1–4, and *AluY* exclusively is shared by APOL1 and APOL2 genes. The sequence-based tree reconstruction argues for a common human–mouse APOL6-like ancestor gene 70 Ma that later diverged into the *AluJ*-orthologous APOL1–4 genes in all investigated

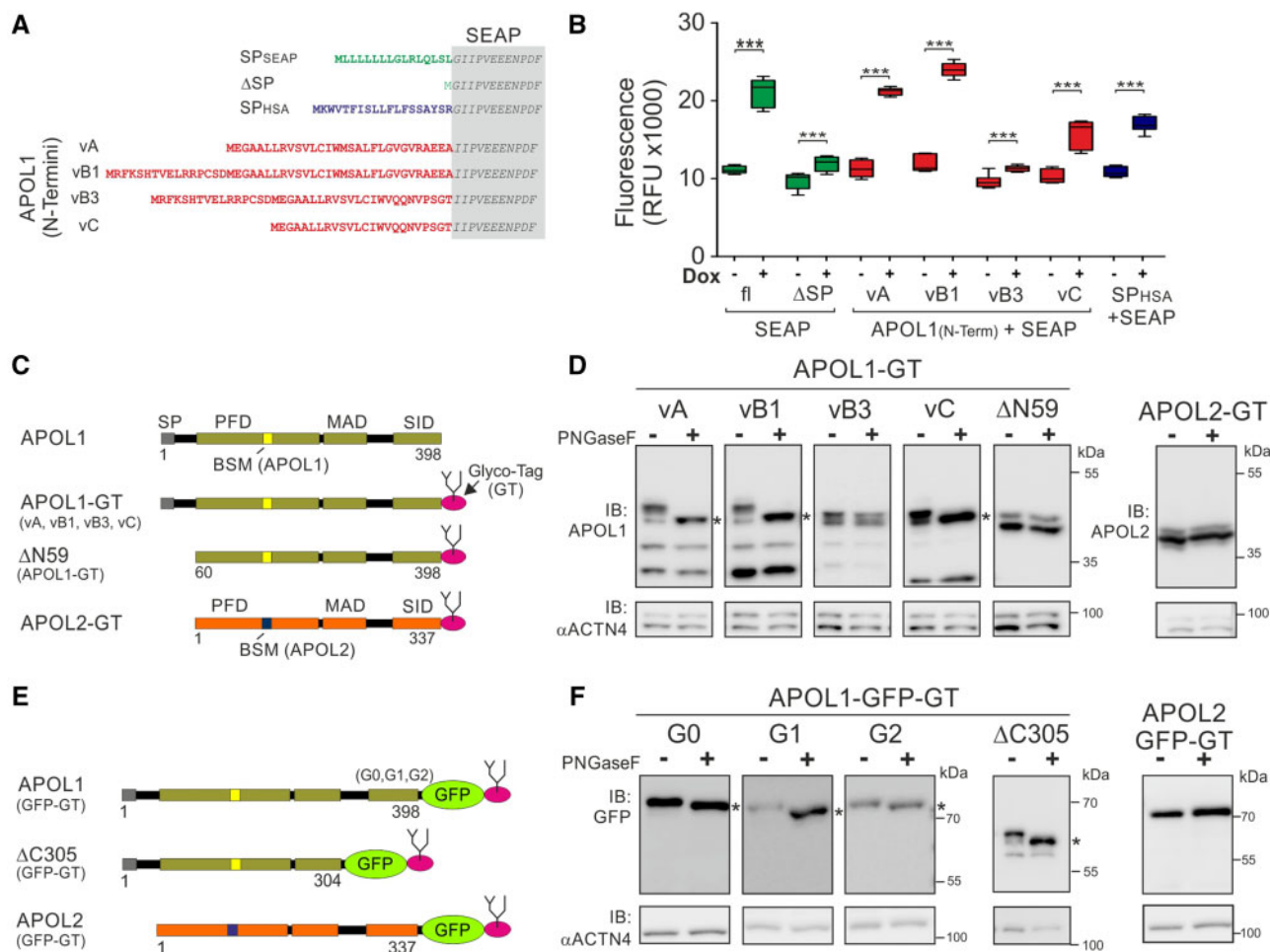


**Fig. 5.** Different ER insertion orientations accompany APOL1–APOL2 diversification. (A) The endogenous SP of the reporter enzyme SEAP (secreted alkaline phosphatase, gray box) was replaced by the N-termini of the APOL1 splice variants (vA, vB1, vB3, vC). The endogenous SP of SEAP (SP<sub>SEAP</sub>) and the well-known SP of human serum albumin (SP<sub>HSA</sub>) served as positive, and SEAP lacking its SP (ΔSP) as negative control. (B) SEAP secretion assay in HEK293T cells. Fluorescent SEAP secretion was detectable for positive controls (SP<sub>SEAP</sub> and SP<sub>HSA</sub>) and splice variants vA, vB1, and vC. SEAP with the N-termini of APOL1 vB3 and without the SEAP SP (ΔSP) were not secreted ( $***P < 0.0001$ ). (C) Scheme: APOL1 splice variants vA, vB1, vB3, vC, a mutant lacking the complete APOL1 N-terminus (aa1–59; ΔN59), and APOL2 were fused with an artificial C-terminal N-glycosylation tag (GT). (D) Western blot analyses of Glyco-tag (GT) APOL proteins (shown in C) before and after PNGaseF glycosidase digestion showed N-glycosylation and therefore ER luminal localization only for APOL1 vA, vB1, and vC (marked by black asterisks). (E) Scheme: C-terminally GFP-tagged APOL1 (G0 and renal risk variants G1 and G2), APOL1 lacking C-terminal aa305–398 (ΔC305), and APOL2. (F) Western blot analysis of these GFP-GT-tagged proteins (shown in E) before and after PNGaseF glycosidase digestion demonstrates luminal ER localization for these proteins (asterisks), except for APOL2-GFP-GT.

primates, followed by the appearance of *AluY*-orthologous *APOL1–2* genes in Old World monkeys (*Catarrhini*). *APOL5* is among the placental precursors of *APOL* genes but removed from the mouse genome. *APOLD1*, on the other hand, predates the mammalian divergence and is still highly conserved in most vertebrates.

Although *APOL2* is found mainly in the brain, the highest expression of *APOL1* is in the liver indicating that divergences of *APOL* genes are linked to organ-specific expression patterns and cell type-specific roles of the various family members. The high expression level of *APOL1* in the liver (Shukha et al. 2017) is remarkable as the liver is the chief secretory organ, releasing many if not most of the blood serum components, including *APOL1* (wildtype) and HPR (haptoglobin-related protein), which are key components of the TLF that confers innate

resistance to all strains of *Trypanosoma brucei*, except for subspecies *Trypanosoma brucei rhodesiense* and *Trypanosoma brucei gambiense* (Genovese et al. 2010; Harrington et al. 2014; Cooper et al. 2017; Shukha et al. 2017; De Simone et al. 2020).

In contrast to their different organ-specific expression pattern, which is most likely due to tissue-specific promoter activities, *APOL1* and *APOL2* mainly localize to the ER on an intracellular level. Taking advantage of live-cell imaging approaches using GFP-tags our data suggest that ER targeting is a common and, therefore, probably evolutionarily conserved feature of these closely related proteins. However, this raises the question how the common intracellular localization of these proteins is linked to their opposite cytotoxic properties.



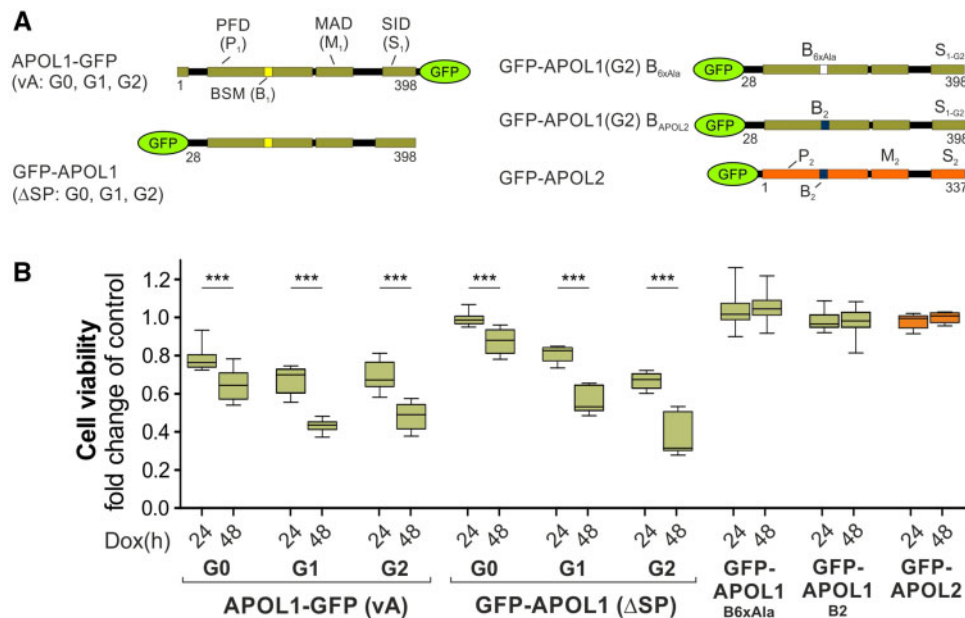


**Fig. 6.** APOL1 cytotoxicity is caused by *cis*- and *trans*-orientated APOL1 pools. (A) Schemes of APOL1 variants used for cell viability assays. *Left panel:* We used APOL1 G0, and renal risk variants G1 and G2 combined with C-terminal GFP (APOL1-GFP, vA aa1–398), and APOL1 fusion proteins (G0, G1, and G2) in which the APOL1 SP was replaced by an N-terminal GFP-tag (GFP-APOL1  $\Delta$ SP; aa28–398). *Right panel:* To analyze the impact of the putative pro-apoptotic “BH3-only motif” (BSM) in APOL1 pools at the outer ER membrane (*trans* orientation), we replaced the BSM of GFP-APOL1 by either an Alanine stretch ( $B_{6xAla}$ ) or the BSM of APOL2 ( $B_2$ ). GFP-tagged APOL2 was used as a control. (B) Cell viability assay of stable HEK293T cell lines expressing proteins summarized in A: APOL1-expressing cell lines, particularly those with RRVs, exhibited cytotoxic effects in *cis* and *trans* orientations. Toxic GFP-APOL1 ( $\Delta$ SP, G2) in which the BSM was replaced by Alanine (GFP-APOL1  $B_{6xAla}$ ) or the BSM of APOL2 (GFP-APOL1  $B_2$ ) and GFP-APOL2 showed no cytotoxicity (\*\*\* $P$  < 0.0001).

The SEAP secretion and Glyco-tag assays used in this study demonstrated that APOL1 variants vA, vB1, and vC are located inside the ER (*cis*), whereas those of vB3 and APOL2 are faced to the cytoplasmic (*trans*) side of the ER. In this context, it is worth noting that the SEAP and glycosylation assays are strongly in line with the APOL1 splice variant orientations elucidated by Scales et al. (2020) using differential permeabilization assays in combination with numerous highly specific antibodies. Thus, evolutionary splitting into APOL1 and APOL2 genes resulted in different ER membranes orientations, but only for three-fourths of the APOL1 splice variants (vA, vB1, and vC). This is of substantial relevance for the various discussed APOL1 pathomechanisms, as it is still discussed whether circulating (meaning secreted) (Hayek et al. 2017) or rather intracellular fractions (in *cis* or *trans* orientation) cause APOL1-linked renal diseases (Bruggeman et al. 2014; Cheng et al. 2015; Heneghan et al. 2015; Khatua et al. 2015; Lan et al. 2015; Ma et al. 2017, 2020; Olabisi et al. 2016; Beckerman et al. 2017; Granado et al. 2017; Kruzel-Davila, Shemer, et al. 2017; Madhavan et al. 2017; Shah et al. 2019; Uzureau et al. 2020).

In a scenario in which APOL1 cytotoxicity requires the SID facing the cytoplasm (fig. 7B, supplementary data SD18, Supplementary Material online), only cytoplasmic APOL1 vB3—or nonprocessed and therefore nonmembrane integrated APOL1 pools—fulfills this criterion. This is in line with studies in which APOL1-cytotoxicity was linked to APOL1 targeting to the outer mitochondrial membrane (Ma et al. 2017), the mitochondrial transition pores (Shah

et al. 2019), mitochondrial fission (Ma et al. 2020), or interactions with Vamp8 (Madhavan et al. 2017) and APOL3 (Uzureau et al. 2020). Moreover, recently Wakashin et al. identified the intracellular NLRP12 (NLR family pyrin domain containing 12)—a key regulator of Toll-like receptor signaling—as a binding partner of the APOL1 vB3 variant. The data suggest a role in which APOL1 vB3 triggers an enhanced podocyte damaging by an upregulated inflammatory signaling (Wakashin et al. 2020).

*Trans* orientated APOL1 also fits the observation that it can bind to phosphoinositides, which are present on the ER's cytoplasmic leaflet (Wan et al. 2008; Chun et al. 2019). Together this indicates that SP-less APOL1 vB3, as well as APOL2 most likely bind peripherally to these lipids (fig. 7B).

The identified BH3-only like sequence motif of APOL proteins points to a similar role in cell programmed death (PCD) scenarios as shown for other members of the Bcl2-family (Vanhollebeke and Pays 2006; Wan et al. 2008; Smith and Malik 2009). Some members have been identified as factors mediating PCD by directly activating Bax/Bak proteins at the outer mitochondrial membrane to trigger apoptosis (Shamas-Din et al. 2011; Dummer et al. 2015; Adams and Cory 2018). Intriguingly, cytoplasmic orientated GFP-APOL1 in which its BSM is replaced by that of APOL2 loses its cytotoxicity (while maintaining ER targeting; fig. 6B, supplementary data SD15, Supplementary Material online). These data suggest a BSM role as cofactor in APOL1-linked cell death (Wan et al. 2008; Lan et al. 2015) and are in line with previous studies that observed mitochondrial damaging in cells



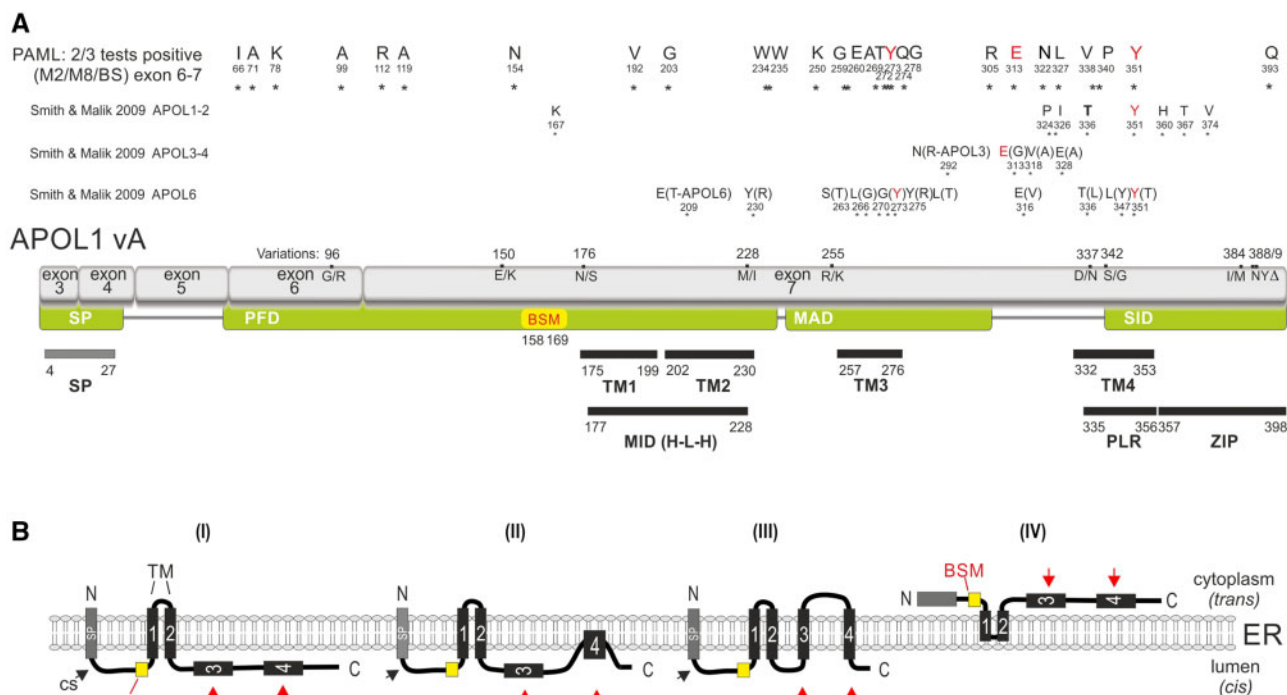


**Fig. 7.** APOL1 vA gene structure and regions with positively selected sites. (A) Amino acids (single letter code) and coordinates mark positively selected sites for APOL1–4 derived from at least two of three PAML models (M2/M8/BS) as large stars. The positively selected sites found by Smith and Malik (2009) are indicated for APOL1–2, APOL3–4, and APOL6. Red labeled letters show overlapping sites of different studies. The APOL1 variation of alternative amino acids or deletion sites ( $\Delta$ ) are shown above the exon structure (gray). APOL1 was previously divided into four functional regions, an SP, a PFD, an MAD, and the SID (green boxes). The PFD also contains a putative pro-apoptotic BH3-only domain sequence motif (BSM). More recent conceptions suggest an SP (gray bar) and up to four TMs (SP, gray and TM1–4, black bars with their coordinates indicated as numbers). The first two TMs are also referred to as membrane insertion domain (MID) or helix–turn–helix region (H-L-H). The TM4 overlaps with a pore-lining region (PLR), followed by leucine-zipper domain (ZIP). (B) Model of possible orientations of APOL1 (and APOL2) at the ER. The presence or absence of the SP determines the orientation of APOL1 splice variants and of APOL2 at the ER. Functional SPs result in a luminal (*cis*) ER localization of the APOL1 C-terminus. If APOL1 functions as an ion pore, this most likely requires two (I), “two and a half” (II), or four (III) TMs (black boxes). During evolution, positively selected amino acids accumulate in regions within, or close to, the putative TM3 and TM4 (red arrows). APOL1 vB3 and APOL2, that lack functional SPs (IV), are most likely bound to the cytoplasmic leaflet of the ER membrane (*trans*). Since *cis* as well as *trans* pools of APOL1 show cytotoxic effects—that are pronounced in the case of renal risk variants—our data suggest the presence of different cellular pathomechanisms.

overexpressing APOL1 (Ma et al. 2017; Shah et al. 2019). Our data elucidated functional SPs for APOL1 vA, vB1 and vC and, therefore, a luminal orientation of these splice variants’ C-termini. Strikingly, such a *cis* orientation agrees with scenarios in which APOL1’s cytotoxic effects are caused by ion channel activity at the plasma membrane (Thomson and Finkelstein 2015; Olabisi et al. 2016; Bruno et al. 2017; Giovino et al. 2020; Schaub et al. 2020), or where APOL1 is acting as a paracrine (meaning secreted) factor (Hayek et al. 2017).

The  $\Delta$ C305-GFP-GT mutant, which lacks the APOL1 SID but contains the SP of variant A and the helix–turn–helix loop of the MID (aa177–228) showed a luminal orientation. These data indicate the presence of a central membrane insertion domain composed of two juxtaposed membrane spanning helices (TM1 and TM2) and suggest that—at least in this mutant—the region between aa257 and aa276 is unable to form a third membrane spanning helix (TM3). From this point of view, the  $\Delta$ C305 mutant supports a current topology concept in which APOL1—in addition to the SP—contains two TMs and a “half-spanning loop” (fig. 7 and Gupta et al. 2020).

In an alternative concept, APOL1 forms an active cation channel by four TMs, including the central membrane insertion domain (MID, aa177–228, TM1, and TM2), a pore-lining region (PLR, aa335–356, or TM4), and an additional TM3 between MID and PLR (aa257–276, see fig. 7 and Giovino et al. 2020; Schaub et al. 2020). In this model, changes of the intracellular pH-values appear to be crucial for APOL1 membrane insertion and channel function. This includes the possibility that proper formation of a third TM may require the C-terminal SID (aa305–398), indicating that only the full-length APOL1 vA can form four TMs. However, in every case, the suggested APOL1 topology concepts are in line with our glycosylation (and secretion) assays. Most positively selected sites during APOL1 evolution are close to or even within the novel postulated TM3 and TM4 (fig. 7A, supplementary data SD16, Supplementary Material online). Remarkably, positively selected sites also include Y351. This tyrosine is crucial for the pH-dependent gating of APOL1-linked ion channel activity (Schaub et al. 2020) or part of a putative half-spanning loop, suggested by Gupta et al. (2020).

The different APOL1-pathomechanisms are finally a consequence of alternative splicing of the *APOL1* gene. Indeed, alternatively spliced transcripts of a gene can regulate various biological processes, and their evolution often led to functional innovation (Bush et al. 2017). Interestingly, the start codon and 5' GT splicing site of alternative exon 2 of *APOL1* (*APOL1* vB1; fig. 2A) that constitute one of the two SP initiation codes of *APOL1* are present in most primate species representatives of *APOL1*–4 genes (supplementary data SD4, Supplementary Material online), but the expression is restricted to *APOL1*. Apart from that, the alternative SP from exon 3 of *APOL1* (*APOL1* vA and *APOL1* vC) is also represented and expressed for *APOL4* (fig. 2A and B; supplementary data SD4, Supplementary Material online). In this context, it is worth mentioning that the rapid evolution of SPs correlates to a relaxed selection on nonsynonymous and synonymous sites in a gene (Li et al. 2009). Thus, gene duplication goes ahead with relaxation from selective constraints and may explain the evolution of the SPs of *APOL1* after divergence from *APOL2*. Therefore, it is tempting to speculate that the ratio between *APOL1* splice variants is part of ongoing evolution.

Under normal conditions, high and efficient *APOL1* secretion may result in low levels of nonprocessed, luminal-faced fractions of *APOL1* at the ER, thereby most likely preventing damaging of the secreting cells. However, an upregulation of *APOL1*, triggered by inflammatory cytokines, may cause an overload of *APOL1* pools at the ER in *cis* and *trans* orientations (Nichols et al. 2015). Thus, ER targeting combined with high expression levels at the ER could be a key determinant in *APOL1*-linked cytotoxicity, particularly in postmitotic cells like podocytes with a very limited self-renewal capacity (Wen et al. 2018).

Recent studies elucidated high *APOL1* expression levels as an essential cofactor for *APOL1*-linked cytotoxicity (O'Toole et al. 2018; Datta et al. 2020). Furthermore, increasing evidence identified ER stress per se as an aggravating or disease-promoting factor for podocyte diseases (Cybulsky 2013, 2017). Thus, *APOL1* pools at the ER combined with their potential to cause ER-linked disturbances might have—as yet—underestimated potentials in explaining why SP-lacking as well as SP-containing *APOL1* (especially of the G1 and G2 RRVs) induce the observed pleiotropic toxic effects in in vitro and in vivo models.

*APOL1*'s pathobiological mechanisms explaining its cytotoxicity in renal cells are still controversially discussed. This study focusses on the evolutionary history of the *APOL* gene family in mouse and human. In addition, it provides experimental data that both *cis* (luminal) as well as *trans* (cytoplasmic) orientations of *APOL1* splice isoforms could be responsible for the wide spectrum of pathogenic mechanisms proposed for podocyte damage leading to kidney disease. However, *APOL1*-linked cytotoxicity depends on many factors, including *APOL1* expression levels, the haplotype, the presence of renal risk variants, its intracellular localization, and most likely also on the ratio between *cis* and *trans* orientated *APOL1* pools. Hence, further studies will be necessary to

address how a renal risk is turned into *APOL1*-linked kidney diseases.

## Materials and Methods

### Phylogenetic Tree and Gene Reconstruction

We extracted all known human and mouse *APOL* genes using the UCSC Gene Sorter (<https://genome.ucsc.edu>, last accessed August 2, 2021). The *APOL* gene family's gene architecture was derived from both species following the graphically visualized genome assemblies of the UCSC Genome Browser (fig. 1A). To reconstruct the evolutionary history of *APOL* genes, we assembled all amino acid sequences from the large homologous exon 7 (corresponding to *APOL1* vA; fig. 2A) in PhyDE (<http://www.phyde.de>, last accessed August 2, 2021). The alignment was optimized using the MUSCLE multiple sequence aligner PhyDE plugin (Edgar 2004). SplitsTree4 (version 4.15.1, Huson and Bryant 2006) was used to reconstruct the phylogenetic tree of *APOL* genes. We used the Character Method ProteinMLdist under the JTT reconstruction model and four gamma categories to derive the gene affiliations shown in figure 1. SplitsTree reconstructs a consensus network that visualizes potential data conflicts by parallelograms. Next, we performed a bootstrap analysis of a random subset of the data with 100 replicates. When 100% of the resampled data sets showed the same split (suggesting solid phylogenetic signals in the original data set), the related branch was labeled with 100 in the consensus network. The tree topology was verified by applying a maximum likelihood analysis in MEGA7 (JTT matrix-based model, discrete Gamma distribution applying four gamma categories, 100 bootstrap replications), and applying a Bayesian inference in MrBayes 3.2 (prset aamodelpr=fixed Jones, lset rates=invgamma Ngammacat = 4, 200.000 generations, burnin 200) (supplementary data SD1–3, Supplementary Material online).

### Detecting Clade-Supporting Insertions of Transposable Elements

To obtain additional information about the relationship and age of different *APOL* genes in humans, we extracted intron, exon, and UTR genomic regions of the human *APOL* genes. To detect diagnostic TE insertions shared among the primate *APOL* genes, we aligned all six conserved *APOL* genes from various primate representatives (human, orangutan, rhesus monkey, baboon, squirrel monkey, mouse lemur). To identify transposed elements, we ran a local RepeatMasking ([www.repeatmasker.org](http://www.repeatmasker.org)). We extracted *Alu* SINEs, which were then inspected for insertion homology using a genomic alignment from the different members of the *APOL* gene family (supplementary data SD4, Supplementary Material online). Such diagnostic elements are inserted before splitting various gene members, and after that, they represent informative presence/absence markers of relationship at their homologous gene positions.

*Alu* SINEs are primate-specific and the most abundant transposed elements in primates, thus uniquely suitable as clade markers to analyze genes and species' evolution (Churakov et al. 2010). Comparative analyses of the

presence/absence patterns of the identified TEs in various primate species enabled us to determine their evolutionary time of insertion.

### Detecting Positive Selection Sites

To detect positively selected sites within protein-coding sequences, we 1) used the PAML site specific model (model = 0, NSsites = 0 1 2 7 8) and a single Newick user tree, and 2) the branch-site model (model = 2, NSsites = 2,  $\omega = 0$  (estimated), initial  $\omega = 1$  labeled 2201 vs.  $\omega = 1$  (predetermined neutral), initial  $\omega = 1$  labeled 2211) (supplementary data SD16, Supplementary Material online). The PAML incorporated Bayes Empirical Bayes analysis determined the probability of positive selection for each codon position (fig. 7).

### Constructs and Cloning

Expression cassettes encoding EGFP-APOL1 G0 lacking the SP (EGFP- $\Delta$ SP APOL1, aa28–398) or encoding full-length APOL1 G0 with a C-terminal EGFP-tag have been described earlier (Granado et al. 2017). Standard site-directed mutagenesis was used to obtain cDNAs encoding for APOL1 G1 (S342G/I384M) and G2 ( $\Delta$ 388N389Y) renal risk variants. Human APOL2, APOL3, and APOL4 cDNAs were cloned using a human cDNA library derived from AB8 podocytes (Duning et al. 2008) and cloned into pEGFP-N1 (BD Clontech), a modified pEGFP-C2 (encoding RFP instead of EGFP), or pENTR-vectors according to the manufacturer's instructions (Thermo Fisher Scientific). For glycosylation analysis, a Glycotag-tag1.4 tail (AAAAAANATVAAASGDVWDI) (Kaup et al. 2011) was fused to the C-terminal part of different APOL constructs via polymerase chain reaction (PCR). Furthermore, APOL2–APOL1 chimeric constructs, as well as APOL1/2 BH3 mutants, were generated using overlapping primers combined with in combination with SOE PCR techniques. All APOL constructs, deletion constructs, mutants, Glyco-variants, and chimeric constructs were cloned into pENTR or pENTR-EGFP vectors and shuttled into a modified pINDUCER21-Puro destination vector as previously described (Schulze et al. 2014). The pSEAP2-Control vector from Clontech (Takara Cat. No. 631717) served as a template for the different SEAP APOL1 splice variant constructs. For the N-termini, different primers were designed whereby the different APOL1 N-termini and the HSA SP were fused to SEAP during PCR, or the SP of SEAP was deleted (SEAP, SEAP $\Delta$ SP, SEAP-vA-cSPcs, SEAP-vC-cSPcs, SEAP-HSA-SP). Via restriction cloning, the amplified DNA was ligated into a Gateway pDONR221 vector (Invitrogen Cat. No. 12536017) and labeled as pENTR after insertion. For APOL1vB1 the pENTR-SEAP-APOL1vA, and for APOL1vB3 the pENTR-SEAP-APOL1vC, constructs served as templates for PCR. The DNA was subsequently cloned into a pENTR-pDONOR via restriction cloning. All SEAP constructs were shuttled in a doxycycline-inducible pInducer21-Puro destination vector (Schulze et al. 2014). pME-mTagBFP-CAAX was a gift from Nicholas Cole (addgene No. 75149; Don et al. 2017). The BFP-CAAX cassette was shuttled into a pQCXIH destination vector via Gateway LR reaction. The mCherry-Sec61 $\beta$  construct (addgene No. 49155) was kindly provided by Gia Voeltz (Zurek et al. 2011). All constructs were verified by DNA

sequencing. Details concerning constructs are summarized in supplementary data SD19, Supplementary Material online. Primer sequences are available from DM and TW.

### Cell Lines and Transient Transfection

HEK293T cells were cultured in standard DMEM medium (Thermo Fisher Scientific) containing 10% fetal calf serum (FCS) and 1% antibiotics and L-glutamine (penicillin/streptomycin) at 37 °C under a 5% CO<sub>2</sub> atmosphere. Human immortalized AB8/13 podocytes (Saleem et al. 2002) were cultured in standard RPMI 1640 medium (Sigma-Aldrich) containing 10% FCS, 1% supplements, and 1% antibiotics (penicillin/streptomycin) at 33 °C under 5% CO<sub>2</sub> atmosphere (Schulze et al. 2017). Transient transfections were performed via calcium-phosphate-based precipitation (Schulze et al. 2014), or via Lipofectamine 2000 as described in the manufacturer's specifications (Thermo Fisher Scientific).

### Generation of Stable Cell Lines

Stable cell lines were generated as previously described (Schulze et al. 2014; Wennmann et al. 2014). Briefly, lentivirus production was performed in HEK293T cells transiently transfected with psPAX2 and pMD2.G helper plasmids and modified pINDUCER21-Puro-plasmids (Meerbrey et al. 2011) encoding the APOL proteins. The virus-containing supernatant was collected and filtered through a 0.45- $\mu$ m sterile filter (EMD Millipore). The virus-containing medium was added to HEK293T and AB8 podocyte cells using one volume of fresh DMEM medium and one volume of the virus-containing filtrate supplemented with polybrene (final concentration 8  $\mu$ g/ml). After 24 h, the virus-containing medium was replaced by fresh medium, and cells were regenerated for a further 24 h. Transduced cells were selected using puromycin (4  $\mu$ g/ml, HEK293T; 2  $\mu$ g/ml, AB8). All established stable cell lines were tested for inducible overexpression of APOL proteins by western blot and immunofluorescence analysis.

### Cell Viability Assays

Real-time cell viability measurements were performed via the RealTime-Glo MT Cell Viability Assay (Promega) according to the manufacturer's instructions. Briefly, 10,000 HEK293T cells in 50  $\mu$ l medium were seeded onto 96-well white bottom plates (Nunc). After adherence, 50  $\mu$ l 2 $\times$  RealTime-Glo enzyme-substrate mix diluted in medium was added to each well either with or without 125 ng/ml doxycycline (Granado et al. 2017). The luminescence was measured using a 37 °C prewarmed microplate reader (TECAN) at the indicated time points. For each cell line, three independent experiments ( $N = 3$ ), including three technical replicates for each  $N$  ( $n = 3$ ), were measured.

### Western Blot Analyses

Western blot analyses were performed as previously described (Schulze et al. 2014, 2017). Briefly, cell lysates were boiled for 5 min, and equal volumes were separated via SDS-PAGE using 8–15% gels (Bio-Rad). Separated proteins were then transferred to a PVDF membrane (EMD Millipore) and incubated in blocking buffer (5% skim milk powder dissolved



in TBS containing 0.05% Tween-20 [TBS-T]) for 1 h at room temperature. The monoclonal GFP antibody (JL-8; #632380) was provided by Takara Bio Europe (Clontech). The antibodies against APOL1 (HPA018885), APOL2 (HPA001078), and  $\beta$ -Tubulin (#T8328) were purchased from Sigma-Aldrich, the antibody against  $\alpha$ -Actinin 4 (#ALX-210–356) was from Enzo/Alexis. Primary antibodies were used 1:1,000 in TBS-T with 5% bovine serum albumin (BSA) and incubated at 4 °C overnight. The membrane was then washed three times with TBS-T and incubated with horseradish peroxidase-coupled secondary antibodies (Jackson ImmunoResearch) diluted 1:3,000 in blocking buffer for 30–45 min at room temperature. After three further wash steps with TBS-T, the signal was detected using the Lumi-Light chemiluminescence detection reagent (Roche).

### Live-Cell Imaging and Microscopy

For live-cell imaging, cells expressing fluorophore-coupled APOL fusion proteins were grown on  $\mu$ -dishes (Ibidi). Labeling of cells with live-cell imaging dyes, ER-Tracker Red Dye (Ex 587 nm/Em 615 nm; #E34250) or MitoTracker Red CMXRos (Ex 579 nm/Em 599 nm; #M7512), was performed according to the manufacturer's specifications (Thermo Fisher Scientific).

Imaging was performed using an Observer Z1 microscope with APOtome 2.0, AxioCam MRm (Zeiss), and EC Plan APOchromat 63 $\times$ /1.40 Oil M27, or EC Plan-Neofluar 40 $\times$ /1.30 Oil DIC M27 objectives, respectively. Alexa Fluor 594-stained proteins and GFP-tagged fusion proteins were detected using the 38 HE EGFP shift-free filter set (Zeiss). Alexa Fluor647-stained proteins and red live-cell imaging dyes were imaged using the 43 HE Cy3 shift-free (Zeiss) or 64 HE mPlum shift-free (Zeiss) filter sets. BFP-CAAX was imaged using the 49 DAPI shift-free Filter (Zeiss). APOtome images were merged using the Fourier filter. Image files in ZVI or CZI format (Zeiss Axiovision software 4.8; Zeiss ZEN 2.3; blue edition) were further processed using ImageJ (<http://imagej.nih.gov/ij/>, last accessed August 2, 2021). For improved visualization of cellular structures, images were smoothed and sharpened using a Gauss Filter (radius = 1) and the unsharp mask filter (radius = 1; mask weight 0.6–0.8). Finally, images were contrast-adjusted and mounted to complex figures using CorelDRAW Graphics suite  $\times$ 6 software (Adobe).

### In Silico Analyses

Alignment of APOL1 (variant A; 398aa; uniprot O14791) and APOL2 (337aa, uniprot Q9BQE5) sequences was performed using the Multalin software (<http://multalin.toulouse.inra.fr/multalin>, last accessed August 2, 2021) (Corpet 1988). Amino acid comparison between APOL1 and APOL2 was observed via protein BLAST (National Center for Biotechnology Information, U.S. National Library of Medicine, 8600 Rockville Pike, Bethesda, MD 20894, USA). Prediction of putative TMs was realized by the TMHMM server2.0 (DTU Bioinformatics; <http://www.cbs.dtu.dk/services/TMHMM/TMHMM2.0bguide.php>, last accessed August 2, 2021) (Sonnhammer et al. 1998; Krogh et al. 2001). The SignalP 5.0 server was used to observe putative SPs (Almagro

Armenteros et al. 2019). APOL gene expression patterns in human organs were analyzed using a database and an evo-devo application tool (<https://apps.kaessmannlab.org/evodevoapp>, last accessed August 2, 2021) recently provided by Cardoso-Moreira et al. (2019)

### Colocalization Analysis

Analysis was performed by using ImageJ. To analyze colocalization between APOL1-EGFP or EGFP-APOL1 and the membrane, labeled with pQXCIH-BFP-CAAX, a mask Image was created. Therefore, the blue channel was duplicated; a threshold called Moments was applied and manually adjusted to remove the background signal. The Coloc2 PlugIn was used to measure the Pearson Correlation Coefficient (PSF 3.0; Pearson's R-value [no threshold]). GraphPad PRISM software was used to visualize the correlation coefficient analysis. Pearson R-values  $\leq 0.4$  were considered as weak or no correlation,  $> 0.4$  until  $< 0.7$  moderate correlation, and  $\geq 0.7$  strong correlation.

### Statistical Analyses

Statistical analyses were performed using GraphPad PRISM software. To test whether the data sets showed a Gaussian distribution, Shapiro–Wilk normality test was performed. Two groups of normally distributed values were compared using the unpaired *t*-test; two groups of not normally distributed values were compared using the Mann–Whitney test. All data sets were pooled from at least three independent experiments. *P*-values of less than 0.05 were regarded as statistically significant.

### SEAP Assay

To analyze the functionality of different APOL1 N-termini, the secretion of the SEAP reporter enzyme was measured. HEK 293T cells were seeded to the same confluence onto six-well plates and transiently transfected with different SEAP gene variants in a pInducer21-Puro system. The pSEAP2-Control vector from Clontech (Takara Cat. No. 631717) was transfected as a positive control. After transfection, cells were induced with doxycycline (125 ng/ml) and incubated for 48 h. Media of cell cultures were taken to measure secreted proteins, and the cells were used to perform western blot analysis. For the measurement, 50  $\mu$ l of vortexed media was added to 250  $\mu$ l of SEAP working solution (36  $\mu$ M 4-methylumbelliferyl phosphate in 50 mM Tris/0.1% BSA buffer, pH 8.0) in a transparent 96-well plate. After 2 min of incubation in the dark, fluorescence was measured in a microplate reader (Infinite M200, Tecan Group Ltd.) for 60 min. For each cell line, three independent experiments (*N* = 3), including three technical replicates for each *N* (*n* = 3), were measured.

### RIPA Lysates

Cells were grown on cell culture plates and washed with cold phosphate-buffered saline (PBS). For cell lysis, cells were transferred on ice and scraped into RIPA buffer (50 mM Tris-HCl pH 7.4, 150 mM NaCl, 1% NP-40, 0.5% Na-deoxycholate, 0.1% SDS) containing complete protease inhibitor (Roche) and Phosphatase Inhibitor Cocktail II and III (Abcam). Cells

were homogenized by shearing force and then sonicated for 10 min. After removing cell debris and nuclei via centrifugation for 15 min at 4 °C and 10,000 × g, supernatants were stored at −20 °C or directly used for PNGaseF digestion.

### PNGaseF Digestion

The membrane orientations of APOLs were elucidated via glycosylation signals of their C-terminal GT-tag. To confirm glycosylation, RIPA lysates were digested with PNGaseF according to the manufacturer's instructions (New England Biolabs). Laemmli buffer was added to the lysates, and for a digestion control, the origin lysate was mixed with an equal volume of a 50:50 mixture of Laemmli buffer and water.

## Supplementary Material

[Supplementary data](#) are available at *Molecular Biology and Evolution* online.

## Author Contributions

D.M. performed most of the experiments, supported by K.F., D.G., A.C.G., V.K., S.M.L., and T.M.A. Evolutionary studies were mainly done by J.S. D.M., K.F., A.C.G., J.S., and T.W. analyzed the data. D.M., H.P., and T.W. designed the study. D.M., J.S., and T.W. prepared the manuscript. All authors approved the final manuscript.

## Acknowledgments

We thank Beate Surmann, Truc Van Le, and Kristin Doctor for excellent technical support, all laboratory members for fruitful discussions, and Dr Gia Voeltz for plasmids. Moreover, we thank Dr Beate Vollenbröcker and Dr Daniela Braun for the critical reading of the manuscript. Finally, we thank the members of EvoPAD for the inspiring discussions of APOL evolution. The work was supported by grants from the German Research Foundation to T.W. (Grant No. DFG WE 2550/3-1) and J.S. (Grant No. DFG SCHM 1469/10-1). K.F. and T.M.A. were supported by the Medical Faculty of the University of Münster (Medizinerkolleg Münster, MedK grant numbers No. 18-80022 and No. 16-0087, respectively). The work contains parts of the PhD thesis of D.M. and the MD theses of K.F. and T.M.A.

## Data Availability

All relevant data are available within this article, the Supplementary Material online, or from the corresponding author upon request.

## References

Adams JM, Cory S. 2018. The BCL-2 arbiters of apoptosis and their growing role as cancer targets. *Cell Death Differ.* 25(1):27–36.

Almagro Armenteros JJ, Tsirigos KD, Sønderby CK, Petersen T N, Winther O, Brunak S, von Heijne G, Nielsen H. 2019. SignalP 5.0 improves signal peptide predictions using deep neural networks. *Nat Biotechnol.* 37(4):420–423.

Beckerman P, Bi-Karchin J, Park ASD, Qiu C, Dummer PD, Soomro I, Boustany-Kari CM, Pullen SS, Miner JH, Hu C-AA, et al. 2017. Transgenic expression of human APOL1 risk variants in podocytes induces kidney disease in mice. *Nat Med.* 23(4):429–438.

Bruggeman LA, O'Toole JF, Ross MD, Madhavan SM, Smurzynski M, Wu K, Bosch RJ, Gupta S, Pollak MR, Sedor JR, et al. 2014. Plasma apolipoprotein L1 levels do not correlate with CKD. *J Am Soc Nephrol.* 25(3):634–644.

Bruno J, Pozzi N, Oliva J, Edwards JC. 2017. Apolipoprotein L1 confers pH-switchable ion permeability to phospholipid vesicles. *J Biol Chem.* 292(44):18344–18353.

Bush SJ, Chen L, Tovar-Corona JM, Urrutia AO. 2017. Alternative splicing and the evolution of phenotypic novelty. *Philos Trans R Soc Lond B Biol Sci.* 372(1713):20150474.

Capewell P, Cooper A, Clucas C, Weir W, MacLeod A. 2015. A co-evolutionary arms race: trypanosomes shaping the human genome, humans shaping the trypanosome genome. *Parasitology* 142(Suppl 1):S108–S119.

Cardoso-Moreira M, Halbert J, Vallotton D, Velten B, Chen C, Shao Y, Liechti A, Ascensão K, Rummel C, Ovchinnikova S, et al. 2019. Gene expression across mammalian organ development. *Nature* 571(7766):505–509.

Chen TK, Choi MJ, Kao WHL, Astor BC, Scialla JJ, Appel LJ, Li L, Lipkowitz MS, Wolf M, Parekh RS, et al. 2015. Examination of potential modifiers of the association of APOL1 alleles with CKD progression. *Clin J Am Soc Nephrol.* 10(12):2128–2135.

Cheng D, Weckerle A, Yu Y, Ma L, Zhu X, Murea M, Freedman BI, Parks JS, Shelness GS. 2015. Biogenesis and cytotoxicity of APOL1 renal risk variant proteins in hepatocytes and hepatoma cells. *J Lipid Res.* 56(8):1583–1593.

Chun J, Zhang JY, Wilkins MS, Subramanian B, Riella C, Magraner JM, Alper SL, Friedman DJ, Pollak MR. 2019. Recruitment of APOL1 kidney disease risk variants to lipid droplets attenuates cell toxicity. *Proc Natl Acad Sci U S A.* 116(9):3712–3721.

Churakov G, Grundmann N, Kuritzin A, Brosius J, Makalowski W, Schmitz J. 2010. A novel web-based TinT application and the chronology of the primate Alu retroposon activity. *BMC Evol Biol.* 10:376. [PMC][10.1186/1471-2148-10-376] [21126360]

Cooper A, Ilboudo H, Alibu VP, Ravel S, Enyaru J, Weir W, Noyes H, Capewell P, Camara M, Milet J, et al. 2017. APOL1 renal risk variants have contrasting resistance and susceptibility associations with African trypanosomiasis. *Elife* 6.

Corpet F. 1988. Multiple sequence alignment with hierarchical clustering. *Nucleic Acids Res.* 16(22):10881–10890.

Cybulsky AV. 2013. The intersecting roles of endoplasmic reticulum stress, ubiquitin-proteasome system, and autophagy in the pathogenesis of proteinuric kidney disease. *Kidney Int.* 84(1):25–33. [PMC][10.1038/ki.2012.390] [23254900]

Cybulsky AV. 2017. Endoplasmic reticulum stress, the unfolded protein response and autophagy in kidney diseases. *Nat Rev Nephrol.* 13(11):681–696. [CrossRef][10.1038/nrneph.2017.129][PMC][28970584]

Datta S, Kataria R, Zhang JY, Moore S, Petitpas K, Mohamed A, Zahler N, Pollak MR, Olabisi OA. 2020. Kidney disease-associated APOL1 variants have dose-dependent, dominant toxic gain-of-function. *J Am Soc Nephrol.* 31(9):2083–2096. [PMC][10.1681/ASN.2020010079] [32675303]

De Simone G, Pasquabisceglie A, Polticelli F, di Masi A, Ascenzi P. 2020. Haptoglobin and the related haptoglobin protein: the N-terminus makes the difference. *J Biomol Struct Dyn.* 1–10. doi: 10.1080/07391102.2020.1837675.

Don EK, Formella I, Badrock AP, Hall TE, Morsch M, Hortle E, Hogan A, Chow S, Gwee SSL, Stoddart JJ, et al. 2017. A Tol2 gateway-compatible toolbox for the study of the nervous system and neurodegenerative disease. *Zebrafish* 14(1):69–72.

Duchateau PN, Pullinger CR, Orellana RE, Kunitake ST, Naya-Vigne J, O'Connor PM, Malloy MJ, Kane JP. 1997. Apolipoprotein L, a new human high density lipoprotein apolipoprotein expressed by the pancreas. Identification, cloning, characterization, and plasma distribution of apolipoprotein L. *J Biol Chem.* 272(41):25576–25582.

Dummer PD, Limou S, Rosenberg AZ, Heymann J, Nelson G, Winkler CA, Kopp JB. 2015. APOL1 kidney disease risk variants: an evolving landscape. *Semin Nephrol.* 35(3):222–236.

- Duning K, Schurek E-M, Schlüter M, Bayer M, Reinhardt H-C, Schwab A, Schaefer L, Benzing T, Schermer B, Saleem MA, et al. 2008. KIBRA modulates directional migration of podocytes. *J Am Soc Nephrol*. 19(10):1891–1903. [PMC][10.1681/ASN.2007080916] [18596123]
- Edgar RC. 2004. MUSCLE: multiple sequence alignment with high accuracy and high throughput. *Nucleic Acids Res*. 32(5):1792–1797.
- Freedman BI, Julian BA, Pastan SO, Israni AK, Schladt D, Gautreaux MD, Hauptfeld V, Bray RA, Gebel HM, Kirk AD, et al. 2015. Apolipoprotein L1 gene variants in deceased organ donors are associated with renal allograft failure. *Am J Transplant*. 15(6):1615–1622.
- Freedman BI, Kopp JB, Langefeld CD, Genovese G, Friedman DJ, Nelson GW, Winkler CA, Bowden DW, Pollak MR. 2010. The apolipoprotein L1 (APOL1) gene and nondiabetic nephropathy in African Americans. *J Am Soc Nephrol*. 21(9):1422–1426.
- Freedman BI, Pastan SO, Israni AK, Schladt D, Julian BA, Gautreaux MD, Hauptfeld V, Bray RA, Gebel HM, Kirk AD, et al. 2016. APOL1 genotype and kidney transplantation outcomes from deceased African American donors. *Transplantation* 100(1):194–202.
- Friedman DJ, Pollak MR. 2011. Genetics of kidney failure and the evolving story of APOL1. *J Clin Invest*. 121(9):3367–3374.
- Genovese G, Friedman DJ, Ross MD, Lecordier L, Uzureau P, Freedman BI, Bowden DW, Langefeld CD, Oleksyk TK, Uscinski Knob AL, et al. 2010. Association of trypanolytic APOL1 variants with kidney disease in African Americans. *Science* (80-) 329(5993):841–845.
- Giovinazzo JA, Thomson RP, Khalizova N, Zager P, Malani N, Rodriguez-Boulant E, Raper J, Schreiner R. 2020. Apolipoprotein L-1 renal risk variants form active channels at the plasma membrane driving cytotoxicity. *Elife*.
- Granado D, Müller D, Krausel V, Kruzel-Davila E, Schuberth C, Eschborn M, Wedlich-Söldner R, Skorecki K, Pavenstädt H, Michgehl U, et al. 2017. Intracellular APOL1 risk variants cause cytotoxicity accompanied by energy depletion. *J Am Soc Nephrol*. 28(11):3227–3238.
- Gupta N, Wang X, Wen X, Moran P, Paluch M, Hass PE, Heidersbach A, Haley B, Kirchhofer D, Brezski RJ, et al. 2020. Domain-specific antibodies reveal differences in the membrane topologies of apolipoprotein L1 in serum and podocytes. *J Am Soc Nephrol*. 31(9):2065–2082.
- Hajduk SL, Moore DR, Vasudevacharya J, Siqueira H, Torri AF, Tytler EM, Esko JD. 1989. Lysis of *Trypanosoma brucei* by a toxic subspecies of human high density lipoprotein. *J Biol Chem*. 264(9):5210–5217.
- Harrington JM, Nishanova T, Pena SR, Hess M, Scelsi CL, Widener J, Hajduk SL. 2014. A retained secretory signal peptide mediates High Density Lipoprotein (HDL) assembly and function of haptoglobin-related protein. *J Biol Chem*. 289(36):24811–24820.
- Hayek SS, Koh KH, Grams ME, Wei C, Ko Y-A, Li J, Samelko B, Lee H, Dande RR, Lee HW, et al. 2017. A tripartite complex of suPAR, APOL1 risk variants and  $\alpha\text{v}\beta 3$  integrin on podocytes mediates chronic kidney disease. *Nat Med*. 23(8):945–953.
- Heneghan JF, Vandrope DH, Shmukler BE, Giovinazzo JA, Raper J, Friedman DJ, Pollak MR, Alper SL, Alper SL. 2015. BH3 domain-independent apolipoprotein L1 toxicity rescued by BCL2 prosurvival proteins. *Am J Physiol Cell Physiol*. 309(5):C332–C347.
- Huson DH, Bryant D. 2006. Application of phylogenetic networks in evolutionary studies. *Mol Biol Evol*. 23(2):254–267. [PMC][10.1093/molbev/msj030] [16221896]
- Kasembeli AN, Duarte R, Ramsay M, Mosiane P, Dickens C, Dix-Peek T, Limou S, Sezgin E, Nelson GW, Fogo AB, et al. 2015. APOL1 risk variants are strongly associated with HIV-associated nephropathy in black South Africans. *J Am Soc Nephrol*. 26(11):2882–2890.
- Kaup M, Saul VV, Lusch A, Dörsing J, Blanchard V, Tauber R, Berger M. 2011. Construction and analysis of a novel peptide tag containing an unnatural N-glycosylation site. *FEBS Lett*. 585(14):2372–2376. [PMC][10.1016/j.febslet.2011.06.010] [21704619]
- Khatua AK, Cheatham AM, Kruzel ED, Singhal PC, Skorecki K, Popik W. 2015. Exon 4-encoded sequence is a major determinant of cytotoxicity of apolipoprotein L1. *Am J Physiol Cell Physiol*. 309(1):C22–C37.
- Kopp JB, Nelson GW, Sampath K, Johnson RC, Genovese G, An P, Friedman D, Briggs W, Dart R, Korbet S, et al. 2011. APOL1 Genetic Variants in Focal Segmental Glomerulosclerosis and HIV-Associated Nephropathy. *J Am Soc Nephrol*. 22(11):2129–2137.
- Kopp JB, Anders HJ, Susztak K, Podestà MA, Remuzzi G, Hildebrandt F, Romagnani P. 2020. Podocytopathies. *Nat Rev Dis Primers*. 6(1):68.
- Kreit M, Vertommen D, Gillet L, Michiels T. 2015. The interferon-inducible mouse apolipoprotein L9 and prohibitins cooperate to restrict Theiler's virus replication. *PLoS One*. 10(7):e0133190.
- Krogh A, Larsson B, Von Heijne G, Sonnhammer ELL. 2001. Predicting transmembrane protein topology with a hidden Markov model: application to complete genomes. *J Mol Biol*. 305(3):567–580.
- Kruzel-Davila E, Shemer R, Ofir A, Bavli-Kertselli I, Darlyuk-Saadon I, Oren-Giladi P, Wasser WG, Magen D, Zaknoun E, Schuldiner M, et al. 2017. APOL1-mediated cell injury involves disruption of conserved trafficking processes. *J Am Soc Nephrol*. 28(4):1117–1130.
- Kruzel-Davila E, Wasser WG, Skorecki K. 2017. APOL1 nephropathy: a population genetics and evolutionary medicine detective story. *Semin Nephrol*. 37(6):490–507. [PMC][10.1016/j.semnephrol.2017.07.002] [29110756]
- Kuryshv VY, Vorobyov E, Zink D, Schmitz J, Rozhdestvensky TS, Münstermann E, Ernst U, Wellenreuther R, Moosmayer P, Bechtel S, et al. 2006. An anthropoid-specific segmental duplication on human chromosome 1q22. *Genomics* 88(2):143–151.
- Lan X, Wen H, Lederman R, Malhotra A, Mikulak J, Popik W, Skorecki K, Singhal PC. 2015. Protein domains of APOL1 and its risk variants. *Exp Mol Pathol*. 99(1):139–144.
- Lannon H, Shah SS, Dias L, Blackler D, Alper SL, Pollak MR, Friedman DJ. 2019. Apolipoprotein L1 (APOL1) risk variant toxicity depends on the haplotype background. *Kidney Int*. 96(6):1303–1307.
- Larsen CP, Beggs ML, Walker PD, Saeed M, Ambruzs JM, Messias NC. 2014. Histopathologic effect of APOL1 risk alleles in PLA2R-associated membranous glomerulopathy. *Am J Kidney Dis*. 64(1):161–163.
- Lee BT, Kumar V, Williams TA, Abdi R, Bernhardt A, Dyer C, Conte S, Genovese G, Ross MD, Friedman DJ, et al. 2012. The APOL1 genotype of African American kidney transplant recipients does not impact 5-year allograft survival. *Am J Transplant*. 12(7):1924–1928.
- Li YD, Xie ZY, Du YL, Zhou Z, Mao XM, Lv LX, Li YQ. 2009. The rapid evolution of signal peptides is mainly caused by relaxed selection on non-synonymous and synonymous sites. *Gene* 436(1–2):8–11.
- Liao W, Goh FY, Betts RJ, Kemeny DM, Tam J, Bay B-H, Wong WSF. 2011. A novel anti-apoptotic role for apolipoprotein L2 in IFN- $\gamma$ -induced cytotoxicity in human bronchial epithelial cells. *J Cell Physiol*. 226(2):397–406.
- Ma L, Ainsworth HC, Snipes JA, Murea M, Choi YA, Langefeld CD, Parks JS, Bharadwaj MS, Chou JW, Hemal AK, et al. 2020. APOL1 kidney-risk variants induce mitochondrial fission. *Kidney Int Rep*. 5(6):891–904.
- Ma L, Chou JW, Snipes JA, Bharadwaj MS, Craddock AL, Cheng D, Weckerle A, Petrovic S, Hicks PJ, Hemal AK, et al. 2017. APOL1 renal-risk variants induce mitochondrial dysfunction. *J Am Soc Nephrol*. 28(4):1093–1105. [PMC][10.1681/ASN.2016050567] [27821631]
- Madhavan SM, O'Toole JF, Konieczkowski M, Barisoni L, Thomas DB, Ganesan S, Bruggeman LA, Buck M, Sedor JR. 2017. APOL1 variants change C-terminal conformational dynamics and binding to SNARE protein VAMP8. *JCI Insight*. 2(14):e92581.
- Meerbrey KL, Hu G, Kessler JD, Roarty K, Li MZ, Fang JE, Herschkowitz JJ, Burrows AE, Ciccio A, Sun T, et al. 2011. The pINDUCER lentiviral toolkit for inducible RNA interference in vitro and in vivo. *Proc Natl Acad Sci U S A*. 108(9):3665–3670.
- Nichols B, Jog P, Lee JH, Blackler D, Wilmut M, D'Agati V, Markowitz G, Kopp JB, Alper SL, Pollak MR, et al. 2015. Innate immunity pathways regulate the nephropathy gene Apolipoprotein L1. *Kidney Int*. 87(2):332–342.
- Olabisi OA, Zhang J-Y, VerPlank L, Zahler N, DiBartolo S, Heneghan JF, Schlöndorff JS, Suh JH, Yan P, Alper SL, et al. 2016. APOL1 kidney disease risk variants cause cytotoxicity by depleting cellular potassium and inducing stress-activated protein kinases. *Proc Natl Acad Sci U S A*. 113(4):830–837.



- O'Toole JF, Schilling W, Kunze D, Madhavan SM, Konieczkowski M, Gu Y, Luo L, Wu Z, Bruggeman LA, Sedor JR. 2018. ApoL1 overexpression drives variant-independent cytotoxicity. *J Am Soc Nephrol.* 29(3):869–879.
- Page NM, Butlin DJ, Lomthaisong K, Lowry PJ. 2001. The human apolipoprotein L gene cluster: identification, classification, and sites of distribution. *Genomics* 74(1):71–78.
- Papeta N, Kiryluk K, Patel A, Sterken R, Kacak N, Snyder HJ, Imus PH, Mhatre AN, Lawani AK, Julian BA, et al. 2011. APOL1 genetic variants in focal segmental glomerulosclerosis and HIV-associated nephropathy. *J Am Soc Nephrol.* 22(11):1991–2137.
- Pays E, Vanhollebeke B, Uzureau P, Lecordier L, Pérez-Morga D. 2014. The molecular arms race between African trypanosomes and humans. *Nat Rev Microbiol.* 12(8):575–584.
- Pays E, Vanhollebeke B, Vanhamme L, Paturiaux-Hanocq F, Nolan DP, Pérez-Morga D. 2006. The trypanolytic factor of human serum. *Nat Rev Microbiol.* 4(6):477–486.
- Pérez-Morga D, Vanhollebeke B, Paturiaux-Hanocq F, Nolan DP, Lins L, Homblé F, Vanhamme L, Tebabi P, Pays A, Poelvoorde P, et al. 2005. Apolipoprotein L-I promotes trypanosome lysis by forming pores in lysosomal membranes. *Science* 309(5733):469–472.
- Raper J, Fung R, Ghiso J, Nussenzweig V, Tomlinson S. 1999. Characterization of a novel trypanosome lytic factor from human serum. *Infect Immun.* 67(4):1910–1916.
- Reeves-Daniel AM, Depalma JA, Bleyer AJ, Rocco MV, Murea M, Adams PL, Langefeld CD, Bowden DW, Hicks PJ, Stratta RJ, et al. 2011. The APOL1 gene and allograft survival after kidney transplantation. *Am J Transplant.* 11(5):1025–1030.
- Regard JB, Scheek S, Borbiev T, Lanahan AA, Schneider A, Demetriades AM, Hiemisch H, Barnes CA, Verin AD, Worley PF. 2004. Verge: a novel vascular early response gene. *J Neurosci.* 24(16):4092–4103.
- Saleem MA, O'Hare MJ, Reiser J, Coward RJ, Inward CD, Farren T, Xing CY, Ni L, Mathieson PW, Mundel P. 2002. A conditionally immortalized human podocyte cell line demonstrating nephrin and podocin expression. *J Am Soc Nephrol.* 13(3):630–638.
- Scales SJ, Gupta N, de Mazière AM, Posthuma G, Chiu CP, Pierce AA, Hötzel K, Tao J, Foreman O, Koukos G, et al. 2020. Apolipoprotein L1-specific antibodies detect endogenous APOL1 inside the endoplasmic reticulum and on the plasma membrane of podocytes. *J Am Soc Nephrol.* 31(9):2044–2064.
- Schaub C, Verdi J, Lee P, Terra N, Limon G, Raper J, Thomson R. 2020. Cation channel conductance and pH gating of the innate immunity factor APOL1 are governed by pore-lining residues within the C-terminal domain. *J Biol Chem.* 295(38):13138–13149. [PMC][10.1074/jbc.RA120.014201] [32727852]
- Schulze U, Vollenbröker B, Braun D, Van Le T, Granado D, Kremerskothen J, Fränzel B, Klosowski R, Barth J, Fufezan C, et al. 2014. The Vac14-interaction network is linked to regulators of the endolysosomal and autophagic pathway. *Mol Cell Proteomics.* 13(6):1397–1411.
- Schulze U, Vollenbröker B, Kühnl A, Granado D, Bayraktar S, Rescher U, Pavenstädt H, Weide T. 2017. Cellular vacuolization caused by overexpression of the PIKfyve-binding deficient Vac14L156R is rescued by starvation and inhibition of vacuolar-ATPase. *Biochim Biophys Acta Mol Cell Res.* 1864(5):749–759. [PMC][10.1016/j.bbmr.2017.02.012] [28216340]
- Shah SS, Lannon H, Dias L, Zhang JY, Alper SL, Pollak MR, Friedman DJ. 2019. APOL1 kidney risk variants induce cell death via mitochondrial translocation and opening of the mitochondrial permeability transition pore. *J Am Soc Nephrol.* 30(12):2355–2368.
- Shamas-Din A, Brahmabhatt H, Leber B, Andrews DW. 2011. BH3-only proteins: orchestrators of apoptosis. *Biochim Biophys Acta.* 1813(4):508–520.
- Shukha K, Mueller JL, Chung RT, Curry MP, Friedman DJ, Pollak MR, Berg AH. 2017. Most ApoL1 is secreted by the liver. *J Am Soc Nephrol.* 28(4):1079–1083.
- Smith EE, Malik HS. 2009. The apolipoprotein L family of programmed cell death and immunity genes rapidly evolved in primates at discrete sites of host-pathogen interactions. *Genome Res.* 19(5):850–858.
- Sonnhammer EL, von Heijne G, Krogh A. 1998. A hidden Markov model for predicting transmembrane helices in protein sequences. *Proc Int Conf Intell Syst Mol Biol.* 6:175–182.
- Thomson R, Finkelstein A. 2015. Human trypanolytic factor APOL1 forms pH-gated cation-selective channels in planar lipid bilayers: relevance to trypanosome lysis. *Proc Natl Acad Sci U S A.* 112(9):2894–2899.
- Tzur S, Rosset S, Shemer R, Yudkovsky G, Selig S, Tarekgn A, Bekele E, Bradman N, Wasser WG, Behar DM, et al. 2010. Missense mutations in the APOL1 gene are highly associated with end stage kidney disease risk previously attributed to the MYH9 gene. *Hum Genet.* 128(3):345–350.
- Uzureau S, Lecordier L, Uzureau P, Hennig D, Graversen JH, Homblé F, Mfutu PE, Oliveira Arcolino F, Ramos AR, La Rovere RM, et al. 2020. APOL1 C-terminal variants may trigger kidney disease through interference with APOL3 control of actomyosin. *Cell Rep.* 30(11):3821–3836.e13.
- Vanhamme L, Paturiaux-Hanocq F, Poelvoorde P, Nolan DP, Lins L, Van Den Abbeele J, Pays A, Tebabi P, Van Xong H, Jacquet A, et al. 2003. Apolipoprotein L-I is the trypanosome lytic factor of human serum. *Nature* 422(6927):83–87.
- Vanhollebeke B, Pays E. 2006. The function of apolipoproteins L. *Cell Mol Life Sci.* 63(17):1937–1944.
- Velez JCQ, Caza T, Larsen CP. 2020. COVAN is the new HIVAN: the re-emergence of collapsing glomerulopathy with COVID-19. *Nat Rev Nephrol.* 16(10):565–567. [PMC][10.1038/s41581-020-0332-3] [32753739]
- Wakashin H, Heymann J, Roshanravan H, Daneshpajouhnejad P, Rosenberg A, Shin MK, Hoek M, Kopp JB. 2020. APOL1 renal risk variants exacerbate podocyte injury by increasing inflammatory stress. *BMC Nephrol.* 21(1):371. [PMC][10.1186/s12882-020-01995-3] [32854642]
- Wan G, Zhaorigetu S, Liu Z, Kaini R, Jiang Z, Hu CA. 2008. Apolipoprotein L1, a novel Bcl-2 homology domain 3-only lipid-binding protein, induces autophagic cell death. *J Biol Chem.* 283(31):21540–21549.
- Weckerle A, Snipes JA, Cheng D, Gebre AK, Reis JA, Murea M, Shelness GS, Hawkins GA, Furdul CM, Freedman BI, et al. 2016. Characterization of circulating APOL1 protein complexes in African Americans. *J Lipid Res.* 57(1):120–130.
- Wei MC, Zong WX, Cheng EH, Lindsten T, Panoutsakopoulou V, Ross AJ, Roth KA, MacGregor GR, Thompson CB, Korsmeyer SJ. 2001. Proapoptotic BAX and BAK: a requisite gateway to mitochondrial dysfunction and death. *Science* (80-.) 292(5517):727–730.
- Wen H, Kumar V, Lan X, Shostari SSMM, Eng JMM, Zhou X, Wang F, Wang H, Skorecki K, Xing G, et al. 2018. APOL1 risk variants cause podocytes injury through enhancing endoplasmic reticulum stress. *Biosci Rep.* 38:BSR20171713.
- Wennmann DO, Schmitz J, Wehr MC, Krahn MP, Koschmal N, Gromnitsa S, Schulze U, Weide T, Chekuri A, Skryabin BV, et al. 2014. Evolutionary and molecular facts link the WWC protein family to hippo signaling. *Mol Biol Evol.* 31(7):1710–1723. [PMC][10.1093/molbev/msu115] [24682284]
- Wiggins RC. 2007. The spectrum of podocytopathies: a unifying view of glomerular diseases. *Kidney Int.* 71(12):1205–1214.
- Xu B, Yang Z. 2013. PAMLX: a graphical user interface for PAML. *Mol Biol Evol.* 30(12):2723–2724.
- Yang Z. 2007. PAML 4: Phylogenetic analysis by maximum likelihood. *Mol Biol Evol.* 24(8):1586–1591.
- Zhaorigetu S, Wan G, Kaini R, Jiang Z, Hu CAA. 2008. ApoL1, a BH3-only lipid-binding protein, induces autophagic cell death. *Autophagy* 4(8):1079–1082.
- Zhaorigetu S, Yang Z, Toma I, McCaffrey TA, Hu CAA. 2011. Apolipoprotein L6, induced in atherosclerotic lesions, promotes apoptosis and blocks beclin 1-dependent autophagy in atherosclerotic cells. *J Biol Chem.* 286(31):27389–27398.
- Zurek N, Sparks L, Voeltz G. 2011. Reticulon short hairpin transmembrane domains are used to shape ER tubules. *Traffic* 12(1):28–41.